Fuel 291 (2021) 120147

Contents lists available at ScienceDirect

Fuel

journal homepage: www.elsevier.com/locate/fuel

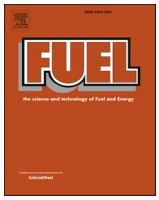

Full Length Article

Detailed examination of the combustion of diesel and glycerol emulsions in a compression ignition engine

David Robert Emberson [a,*], Jan Wyndorps [b], Ahfaz Ahmed [a], Karl Oskar Pires Bjørgen [a], Terese Løvås [a]

[a] Department of Energy and Process Engineering, Norwegian University of Science and Technology, Trondheim, Norway
[b] Institute for Combustion Technology, RWTH Aachen University, Aachen, Germany

ARTICLE INFO

Keywords:
Glycerol
Diesel-engine
Combustion
Soot
Particulate matter
Fuel-additives

ABSTRACT

This study examines glycerol as an additive to diesel fuel to demonstrate it has the potential to suppress the formation of soot/PM. The investigation of a diesel/glycerol emulsion included an engine trial, high-speed imaging in an optical combustion chamber and a fundamental chemical kinetic study examining soot precursor formation. The emulsion had a longer ignition delay but higher AHRR with increasing load. There was no impact on the brake thermal efficiency. CO and THC were higher with the emulsion at the lower engine loads. The emulsion emitted a smaller number of particles with diameters greater than 25 nm, with a significant drop in the number of particles at 60 nm. The number of particles with diameters greater than 25 nm is reduced by 61% at 20 Nm, by 56% at 80 Nm, and by 11% at 140 Nm. A large peak of sub 10 nm particles, 2 orders of magnitude greater than with diesel alone, was observed, hypothesised to be semi-volatile organic compounds that have started to condense. A thermogravimetric analysis supported a larger semi-volatile content. Ignition delay time, determined from the OH* flame emission, was always longer for the emulsion at all conditions. In-flame soot was always lower with the emulsion at all conditions. Flame lift-off length decreased with increasing temperature and pressure of the ambient gas whilst soot increased. The concentration of known soot precursors, C2H2 and C2H4 was reduced but the concentrations of C3H6 and PC3H4 were not significantly affected.

1. Introduction

Particulate matter (PM) emissions from compression ignition (CI) engines pose a considerable environmental and public health problem. Whilst PM emissions from the latest CI equipped vehicles are effectively controlled using diesel particulate filters (DPF), their application on heavy duty vehicles introduces additional maintenance schedules, costs associated with over-sizing and their introduction to larger CI engines (i.e locomotive or marine) is moving at a slower pace [1]. Soot emissions represent the main portion of PM and can be reduced using oxygenated fuels; the presence of oxygen in the fuel aids the soot oxidation process and changes the structure of the soot in a way that facilitates oxidation [2,3]. This means it is worth while to investigate potential oxygenated-fuel-additives for use in large CI engines with the goal to reduce soot emissions. Such additives should reduce soot, be inexpensive, environmentally benign and be readily available to the fuel producer or end user.

European pump diesel, meeting the standard EN590, allows for up to 7 w% first generation biodiesel (often referred to as B7), in the form of a fatty acid methyl ester (FAME), usually made from rapeseed oil (Europe only). FAME is an oxygen containing fuel and is referred to as an oxygenated fuel. The use of oxygenated fuels in CI engines has been studied extensively and shows a general trend of reducing PM emissions, usually attributed to the oxygen content in the fuel [4]. This effect has been observed in studies examining in-flame soot production [5–7] and engine out emissions [4,8–10], though size distribution of the PM in the exhaust is not commonly reported [11]. There is some evidence that the use of FAME may reduce PM mass but lead to a change in the size distribution [12]. If there is an increase in the smaller sizes of PM, which are more harmful to human health, the perceived benefit of PM mass reduction may be negated.

FAME is produced by the transesterification process where vegetable oil feed-stock is reacted with an alcohol (often methanol) in the presence of a catalyst, producing a mixture of fatty acid esters and roughly a 10%

* Corresponding author.
E-mail address: david.r.emberson@ntnu.no (D.R. Emberson).

https://doi.org/10.1016/j.fuel.2021.120147
Received 24 March 2020; Received in revised form 20 October 2020; Accepted 4 January 2021
Available online 9 February 2021

yield of glycerol (1,2,3-Propanetriol). This glycerol is refereed to as crude glycerol and will contain many impurities associated with the transesterification process [13]. Glycerol is the pure chemical compound 1,2,3 propanotrial, while "glycerin" usually applies to a purified commercial product with contents of higher than 95% glycerol. Many grades of glycerin are commercially available; obtained after removal of salts, methanol, and free fatty acids. In most commercial applications the quality of glycerin must be improved until it has an acceptable purity that is completely different from those obtained in biodiesel facilities [14].

With the increase in the volume of FAME production over the last decade, the production of crude glycerol has also significantly increased and now exceeds the demand [15,16]. Glycerol/glycerin has several industrial uses but its use as a fuel additive, given its high oxygen content and the advantage of a short closed product cycle is considered in this study. Glycerol has been shown to be usable as a combustion fuel directly [17] but is most likely to be considered as an engine fuel in the form of blend with a standard fuel; however, in its pure form it is immiscible with diesel and has a much higher viscosity. There are studies examining upgraded products of glycerol: glycerol carbonate; solketal and; triacetin, to use in fuel blends [18–22] to bring the viscosity within diesel range and to improve their miscibility with diesel. In previous studies examining glycerol as a fuel additive, the glycerol was utilized by forming diesel (or biodiesel) and glycerol emulsions.

In Sidhu et al. [23] CI engine trials with diesel–biodiesel blends and glycerin emulsions, using biodiesel and glycerin produced from a laboratory-scale biodiesel production, with glycerin purification, were examined. Emulsions were produced using a high-shear force blender and a surfactant mixture of Span 80 and Tween 80 with hydrophilic-lipophilic balance (HLB) of 6.4. Viscosity measurements shown that by using glycerol in the form of an emulsion the issue of its very high viscosity can be avoided. NOx emissions increased with increasing the biodiesel percentage in the blends but reduced with the increase in the percentage of glycerin in the emulsions. The largest reduction in NOx was observed at the highest engine load tested, with the average NOx of the biodiesel 10% glycerin emulsion being 18% lower than that of pure biodiesel and more than 10% lower than pure diesel. A decrease was seen in the "smoke" levels (measured with a SMART 2000 opacity meter) with the addition of glycerin. The biodiesel 10% glycerin emulsion reduced the observed smoke by 53% compared with the pure biodiesel. Carbon monoxide and total unburned hydrocarbon (THC) declined with the increase in biodiesel but increased in the case of glycerin emulsion. The pure biodiesel emitted 16% lower CO than the pure diesel and there was no change in the CO emissions with up to biodiesel 5% glycerin emulsion. Pure biodiesel emitted 40% lower THC than pure diesel; biodiesel 5% glycerin emitted 10% lower THC than pure diesel.

Eaton et al. [24] conducted engine trials with diesel/glycerol emulsions. Based upon the stability tests conducted, a 10 vol% and a 20 vol% diesel/glycerol emulsion was prepared using a surfactant mixture of Span 80 and Tween 80 (HLB = 6) at a concentration of 1 vol%. The emulsions were made using an ultrasonic homogeniser with the earliest complete emulsion separation occurring after 42 h. Combustion testing was conducted in a naturally aspirated engine at 900 rpm with no adjustment to combustion phasing. A nominal combustion delay was observed with the emulsions which was accounted for by the lower cetane rating compared to the pure diesel. The emulsions increased thermal efficiency at the high engine loads with reductions in NOx and PM emissions of 5–15 and 25–50%, respectively. PM reductions were most pronounced at high load, where fuel-rich zones become prevalent in the cylinder. At the lower loads the PM emissions were equivalent for all fuels. CO and THC were prevalent during low-load operation with CO emissions elevated for glycerol fuels at low engine loads.

McNeal et al. [25] conducted trials of pure glycerol in a CI engine, the work concluded that a heated intake of 90 °C is required to promote ignition inside the combustion chamber, due to glycerol's high ignition energy. The engine also emitted higher quantities of CO due to incomplete combustion, resulting in a lower engine efficiency. Whilst there are some indications diesel/glycerol emulsions may have positive effects, there is a lack of work examining their combustion in a CI engine and their emissions, especially the size distribution of the PM and the in-cylinder soot production.

This study aims to explore the combustion characteristics of a diesel/glycerol emulsion in compression ignition conditions. Analysis is conducted using; an instrumented engine fitted with an emissions analyzer and a differential mobility spectrometer, an optically accessible compression ignition combustion chamber (OACIC) for in-cylinder soot formation examination and; a chemical kinetic study using Chemkin to examine effect of glycerol addition on soot precursors.

The work stems from the hypothesis that glycerol could be used as an oxygenated fuel additive to reduce soot, that it is low cost, environmentally benign and finds a use for the over-supply of glycerol from biodiesel production and reduces soot. The authors do not consider the development of diesel/glycerol emulsions as a drop in fuel to replace diesel fuel in light and medium duty vehicles but as an on board, in situ method to introduce an additive that reduces soot and PM under certain conditions for heavy duty, large CI engines; thus reducing the loading on the DPF or maybe introducing soot and PM that is useful for a DPF regeneration cycle. To truly represent the glycerol produced as a byproduct from the biodiesel industry, crude glycerol, containing a mixture of glycerol, water, salt and methanol should be used, or at a minimum, a moderately processed crude glycerol (glycerin). The use of crude glycerol would impact the combustion, emissions and engine components. i.e higher levels of corrosion. At this initial stage of testing of the hypothesis, the main goal was to examine the efficacy of glycerol (alone) as a fuel additive; its impact on soot and an attempt to use a basic chemical kinetic study to support some of the observations, therefore, refined glycerol was used, to remove the impact of other components that would be present in real crude glycerol.

2. Methods

2.1. Fuels

Glycerol is immiscible with diesel, hence diesel/glycerol emulsions were prepared using a mixture of the surfactants Span 80 and Tween 80 with a lipophilic–hydrophilic balance of HLB = 6.4, as suggested by Sidhu [23]. A 15 w% glycerol emulsion (G15 hereafter) with a surfactant fraction of 1.14 w% was produced. An EN 590 reference diesel (Coryton Fuels) was used for the emulsion diesel fuel and as the baseline fuel for comparison, DRef hereafter. The relevant fuel properties are shown in Table 1. The glycerol used was food grade, 99% pure (Sigma Aldrich, CAS-56–81-5).

Due to the design and operation of the common rail injection system installed on the engine there is a very high fuel flow rate to high pressure

Table 1
Reference diesel and glycerol properties.

Property	Ref Diesel	Glycerol
chemical formula	$C_{11-14}H_{22-28}$ [a]	$C_3H_8O_3$
oxygen ratio[b] [%]	0	30
specific gravity [g/ml]	0.823[a]	1.26[c]
kinematic viscosity [cSt]	2.53[a]	270[d]
lower heating value [MJ/kg]	43.3[a]	16.06[e]
cetane number	60.4[a]	5[f]
initial boiling point [°C]	212[a]	290[c]
flash point [°C]	90.5[a]	177[c]

[a] reference diesel analysis, supplied with fuel,
[b] Described in [6],
[c] glycerol data sheet, supplied from manufacturer,
[d] measured,
[e] from Sidhu [23],
[f] from Setyawan [26]

pump, the common rail and the injectors that is unused and returned to the tank, via a water cooled heat exchanger. Hence the fuel in the tank is subject to continuous, very high shear mixing in the engine's fuel system. For engine testing, approx. 12 liters of fuel was required. The emulsion was made by first mixing the diesel, glycerol and surfactant in approx 4 liter batches using a magnetic stirrer. Ultrasonic mixing of these larger volumes was not possible due to the limited size of the ultrasonic mixer available. This initial emulsion was then added to the engine fuel tank where the final emulsification was done by the fuel circulating, high shear mixing fuel system. Samples of the emulsion were taken for stability and viscosity measurements.

For the OACIC testing, no such fuel return flow is present in the system due to the difference in the high pressure injection system used. The OACIC required approx. 300 ml of emulsion for a complete test. The emulsion for the OACIC testing was produced with ultrasound [27] using a Hielscher UP200Ht for a period of 5 min at a rate of 200 W. To ensure that emulsions for engine and OACIC were comparable, the two emulsions were initially compared visually and their viscosity's were measured; visually the emulsions looked identical and the measured viscosity for each emulsion was also the same, hence the emulsions were determined to be very similar for each test. The stability was assessed by placing a small volume of the emulsion in a 10 ml measuring cylinder. Both emulsions exhibited similar stability, with the emulsion starting to break after approx 30 min. This was much shorter time than that experienced in the works by Sidhu and Eaton [23,24] but long enough for the test in the OACIC to be conducted. Separation was not a problem in the engine test due to the continual mixing. This difference is most likely due to the reference diesel used in this study.

The oxygen ratio is chosen in order to compare different oxygenated fuels regarding their oxygen content, introduced by Mueller et al. [6]. Ω_f represents the percentage of oxygen required for complete combustion that is already supplied by the oxygen bound in the fuel and is defined as the ratio between the oxygen present in the fuel and the amount of oxygen needed to convert all the carbon and hydrogen in the fuel into carbon dioxide and water (Eq. 1). Unlike the oxygen weight or molar percentage, this parameter takes the fuel composition into account as hydrogen and carbon demand oxygen differently.

$$\Omega_f = \frac{n_O}{2n_C + 0.5n_H} \tag{1}$$

The glycerol content was selected with regard to the properties of biodiesel which has an oxygen ratio of approximately $\Omega_f = 3.7\%$. The G15 features a heating value and an oxygen ratio comparable to a 70% biodiesel diesel blend. The glycerol concentration was also chosen with consideration to functional combustion conditions given then ignition character of glycerol. Table 2 shows the composition of the fuels used, Table 3 shows some important properties of the fuels.

Table 2
Fuel composition.

Component	DRef	G15
Reference Diesel [w%]	100	84.60
Glycerol [w%]	0	14.2
Surfactant Mixture [w%]	0	1.14

Table 3
Fuel properties.

Property	DRef	G15
specific gravity [g/ml]	0.823[a]	0.867[b]
kinematic viscosity [cSt]	2.534[a]	3.55[c]
lower heating value [MJ/kg]	43.33[a]	39.40[b]
oxygen ratio d [%]	0	2.46

[a] Supplied
[b] estimated
[c] measured

2.2. Test engine and instrumentation

The engine used for experimentation was a 6 cylinder, 3.2 liter Mercedes OM613, detailed in [28,12]. The engine gaseous emissions were measured with a Horiba Mexa and the particulate was measured with a Cambuston DMS 500. The engine was operated at a fixed speed of 1800 rpm and 5 loads, specified by the brake torque: 20, 50, 80, 110 and 140 Nm (140 Nm is 35% of maximum torque of the engine, limited by the dynamometer at this speed). The engine is fitted with a variable vane turbocharger which was set at minimum boost for these experiments to maintain intake pressure at atmospheric pressure. Fuel injection pressure was maintained at 650 bar with one single injection. The injection timing for each condition and fuel was changed so as to maintain a 50% cumulative heat release (CA50) at 1 crank angle degree (CAD) after top dead center. This application of constant combustion phasing differs from previous works [24,23,29] where fixed SOI has been used. This combustion phasing is quite early and would not be practical for an engine in real world operation; it was chosen as a balance between the measured PM, NOx and CO; the CO level was very high at lower loads when using the G15.

2.3. The OACIC

Details of the OACIC and measuring techniques are reported in previous works [30]. The OACIC is based on a single cylinder CI engine, with the head redesigned to provide line-of-sight optical access of 50 mm in diameter, see Fig. 1 and Table 4. The OACIC is driven by an electrical motor running at a constant speed of 500 rpm. The intake air is compressed by a Roots compressor and heated by an electrical heater. The intake pressure and temperature are controlled according to a calculated set point.

The thermodynamic conditions in the OACIC were chosen such that the ambient gas density at TDC was constant for all conditions by varying the inlet air temperature and pressure. The thermodynamic conditions were calculated based on a first law model together with ideal gas law including the effect of heat transfer. This allowed the ambient gas conditions to be determined; the ambient gas refers to the trapped air mass that is in the chamber at the start of injection i.e. is ambient to the fuel spray. Based on a first law model, the inlet temperatures and pressures needed to get a varying ambient gas temperature for a constant density of ~16.7 kg/m^3, were found. Table 5 shows the thermodynamic state of the three conditions (Cond.1, Cond.2 and

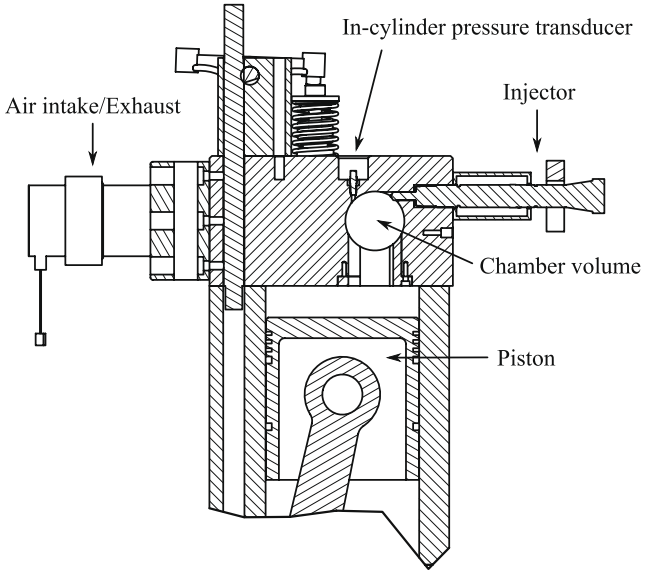

Fig. 1. The OACIC.

Table 4
Specifications of the OACIC.

Engine type	4-stroke, single-cylinder, indirect injection
Bore/Stroke	130 mm/140 mm
Displaced volume	1.85 L
Compression ratio	15.9
Injector	Bosch CR second generation
Injector nozzle	Single hole, DSLA124P1659 62° central axis
Hole diameter	0.12 mm
Injection pressure	1000 bar
Injection duration	4.48 ms
Injection timing	2.7° before TDC

Table 5
Thermodynamic conditions used in the OACIC.

	Cond.1	Cond.2	Cond.3
P Inlet [bar]	1.242	1.406	1.550
T Inlet[K]	328	365.5	408
P TDC [bar]	38.62	41.67	44.63
T TDC [K]	808.0	871.9	933.7
ρ TDC[kg/m^3]	16.65	16.65	16.65

Cond.3) used in this study.

Fuel was injected at 1000 bar, with the start of injection 4 CAD bTDC, which resulted in ignition occurring around TDC for the Cond.1 and at 2 CAD bTDC for Cond.3. The injection duration was 4 ms (12 CAD) which resulted in a steady spray flame being captured. For each fuel and condition, 30 injections, split into three runs of 10 injections each were recorded. A skip-fire mode with 10 non-combustion cycles was used to avoid influence from previous cycle residual gases.

The injected fuel mass and the injected energy was not constant when varying the fuel. To ensure that differences in soot behaviour was not caused by considerable differences in injected energy, the fuel mass injected (for 1000 injections) for each fuel was measured to determine the difference in injected energy. The difference in energy injected for the G15 compared to the reference diesel is −2.9%.

2.4. Optical diagnostics

2.4.1. Diffuse back-illuminated extinction imaging

In-flame soot is determined using diffuse back-illuminated extinction imaging (DBIEI). The technique is based on the principle of light extinction where incident light is absorbed or scattered by particles in the optical path. The resulting transmitted light intensity is therefore lower than the incident light intensity, where transmittance is defined as the ratio between transmitted and incident light intensity. The technique is defined by Beer–Lambert Law, Eq. 2.

$$\tau = \frac{I_t}{I_0} = exp\left(- \int_L k(x)dx \right) = exp(- KL) \tag{2}$$

where τ is the transmittance, I_t is transmitted light intensity, I_0 is incident light intensity, L is the path length through the soot particle cloud and K is the path averaged dimensional extinction coefficient; KL is the optical depth. Using optical and physical properties of soot, the soot volume fraction, the volume of soot and the soot mass can be determined; full details of this calculation are included in [30] but briefly described here. Soot volume fraction is given by Eq. 3.

$$f_v = \frac{\lambda K}{k_e} \tag{3}$$

where f_v is the soot volume fraction, λ is the wavelength of the light and k_e is the dimensionless extinction coefficient. K is calculated from the light extinction measurement and the path length L, k_e is given as $k_e = 6\pi E(m)(1 + \alpha_{sa})$, where $E(m)$ is the imaginary part of the refractive index function (m is the complex refractive index of soot) and α_{sa} is the scattering-to-absorption ratio for the soot measured. For diesel combustion, α_{sa} is often assumed to be zero. The Engine Combustion Network (ECN) recommends $k_e = 7.2$ for light extinction measurements of soot in the wavelength of 628 nm. The recommendation is valid for a diesel-like spray combustion during the quasi-steady period. The estimated uncertainty of k_e is ±20%. Based on Eq. 3, the volume of soot can be calculated by knowing the total measured volume. Since the measurement is performed using a CMOS sensor, KL is measured by a grid of pixels, each having a projected pixel area ΔA_{px}. The projected pixel area times the optical path length through the soot cloud results in the total volume $L\Delta A_{px}$. Multiplying the total volume with the soot volume fraction, yields the soot volume, where the soot mass (m_{soot}) can be calculated from knowing the density of soot (ρ_{soot}).

$$m_{soot} = \rho_{soot} \frac{\lambda \cdot KL}{k_e} \Delta A_{px} \tag{4}$$

The density of soot varies within the flame, where nascent soot is lighter than mature soot, Choi et al. [31] measured the density to be close to 1.8 g/cm^3 which has been used in this study.

2.4.2. Optical setup

The DBIEI optical setup is shown in Fig. 3 and described in more detail, along with the techniques used in [32,30]. The light source was a pulsed, red light-emitting diode (LED). The LED was pulsed with a duration of 1.3 μs. The light from the LED was collimated via a focusing lens on to a large engineered diffuser (diameter of 100 mm) with a spreading angle of 15°. Beam steering effects related to the spatial and angular light intensity distribution from the engineered diffuser are addressed in [32] for the current setup.

The incident (I_0) and the transmitted light intensity distribution (I_t) were measured using a Photron FASTCAM SA5 high speed camera fitted with a Nikkor 50 mm f/1.2 and a 500D close-up lens, a narrow bandpass filter (centered at 630 nm with 10 nm FWHM) and neutral density filters operated at a rate of 100,000 frames per second (fps), with an exposure duration of 1 μs. I_0 was measured with no flame present, i.e. a motored cycle prior to the combustion cycle. During the combustion cycle, the measurement of the backlight (I_t) is strongly influenced by the flame luminosity (I_f) as it is collecting the sum of the two, i.e. $I_{tf} = I_t + I_f$. Since it is the I_t that is of interest, the flame part of the total radiation intensity must be extracted from the recorded data. In this study, this was achieved by measuring I_f only, using alternating frames with no LED pulse. A detailed description of the technique can be found in Bjørgen et al. [32].

Random signal noise (none zero intensity level) is overlaying all intensity signals and can not be distinguished from the real intensity. In high-sooting conditions, the transmitted intensity I_t is close to zero but the noise can cause negative values for the measured transmitted intensity. This effect is illustrated by the shaded area in Fig. 2, on the left side and can occur for a nominal KL value greater than 3.1 with the present setup. If the measured transmitted intensity is negative, a KL value, i.e., a soot concentration can not be determined and the pixels are assigned not-a-number (NaN) in Matlab. An example image is displayed on the right side where KL cannot be calculated and there are dark spots in the middle of the combustion plume, this is referred to as KL saturation.

Instantaneous chemiluminescence from short-lived exited-state OH (OH*) is indicative of high temperature and stoichiometric combustion conditions in the flame [33]. A high speed measurement of the OH* distribution gives a measure of when and where high temperature combustion starts, and the instantaneous flame lift-off length (FLOL). The latter is closely related to in-flame soot formation [33]. The OH* distribution was measured using a Lambert Instruments gated intensifier

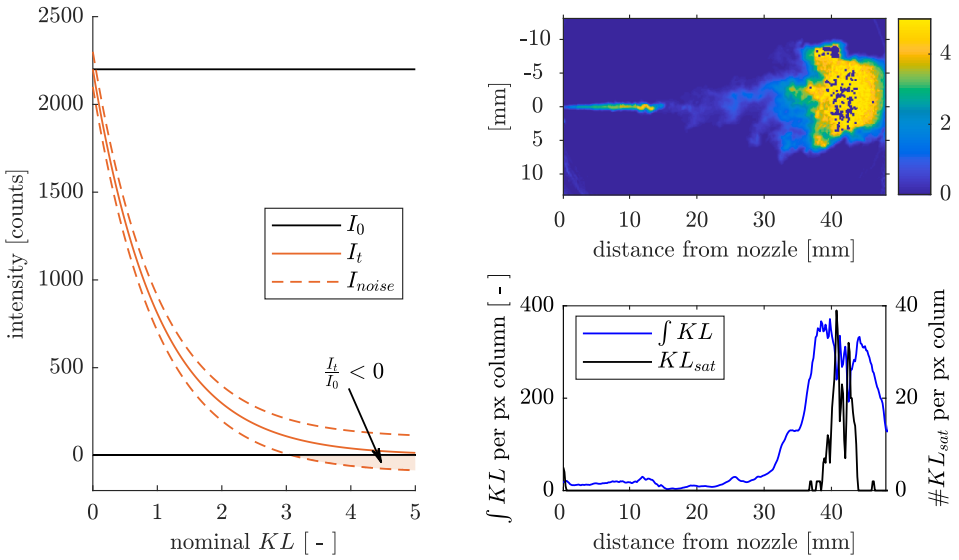

Fig. 2. left: transmitted intensity plotted over nominal KL with the shaded area representing negative measured I_t; right top: example image with KL saturation; right bottom: cross-sectional integrated *KL* and number of KL_{sat} pixels per column.

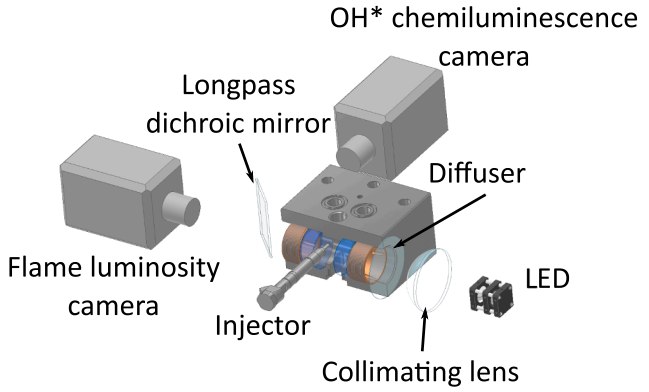

Fig. 3. Experimental optical arrangement around the OACIC.

(II25) fitted to a Photron FASTCAM SA-X2 with a spectral filter centered at 310 nm (BW 10 nm) and a quartz 105 mm UV-Nikkor objective lens. The measurement was synchronized to half the speed of the DBIEI camera, i.e. 50 kfps, in order to match the light extinction measurement frame rate. The same field of view as the DBIEI setup was captured by using a dichoric mirror, reflecting light with shorter wavelength than 480 nm and transmitting longer wavelengths to the DBIEI measurement setup.

2.5. Chemical kinetic analysis

To gain a kinetic understanding of glycerol as a soot mitigating agent, a fundamental approach to elucidate diesel engine combustion, as earlier implemented by Westbrook et al. [34], utilizing homogeneous constant pressure ignition calculations, was conducted. Homogeneous constant pressure reactor cases were run with both the fuels to observe the evolution of soot precursors such as ethene (C2H4), ethyne (C2H2), propene (C3H6) and propyne (PC3H4) during the combustion process and the concentrations of these species long after the ignition event. During simulations, n–heptane was chosen to represent diesel as a surrogate fuel and for cases with glycerol, 15 w% glycerol is added to the n–heptane, similar to the experiments. The soot precursor concentrations were analyzed comparatively for cases with and without glycerol. The hypothesis behind this approach is to simulate the chemical processes leading to ignition, starting from the point where the gas phase reactions start after the evaporation and mixing of fuel and air, and then observe the suite of species which then promote soot inception. The soot precursors were outlined by Westbrook et al. [34] and were originally identified from Frenklach and Wang [35]. The condition at which the simulations were conducted are representative of TDC conditions in OACIC, i.e 40 bar, 770 K, and equivalence ratio of 4 (typical value at flame lift off length [30]). The mechanism used for the study is generated by merging the glycerol mechanism from Hemings et al. [36] and with n–heptane mechanism from Curran et al. [37].

3. Results and discussion

3.1. Engine results

The mean in-cylinder pressure for a minimum of 30 combustion cycles is illustrated in Fig. 4, which shows in-cylinder pressure along with the apparent heat release rate (AHRR) vs. CAD. The solid vertical lines show the start of injection (SOI) for the two fuels. The heat release rate is calculated based on the engine's geometric specifications and a constant ratio of the specific heats of $\gamma = 1.28$. At high engine loads, due to the CA50 timing chosen, the initial heat release advances beyond what would usually be accepted in the operation of an engine (noise and efficiency standpoint) but this does not affect the comparison analysis made between the fuels. The G15 fuel is injected earlier at the lower loads. As the load is increased, G15 injection time approaches the DRef injection time; at the highest load, the G15 is actually injected slightly after the DRef. Also with increasing the load, the G15 fueling resulted in a retarded initial heat release, but a fast heat release (steeper pressure rise). As previous works examining glycerol emulsions in engines did not apply any combustion phasing adjustment [23,24] there is no direct comparison to be made to previous works. Yang et al. [38], when using an emulsion containing some glycerin, observed a later heat release (increased ignition delay) and higher heat release rate when a constant SOI was applied.

This result is highlighted in Fig. 5 which shows the time (in CAD) between the start of injection (SOI) and the CAD of 10% cumulative release (CA10, the ignition delay) and the CAD of 50% cumulative release (CA50). This shows that as the load increases, the ignition delay decreases for both fuels, due to the higher temperatures present, and with increasing load the time to CA50 increases with DRef, which is to be expected as the volume of fuel injected is increasing but this time to CA50 for the G15 reduces, signifying the burn rate of the G15 increases

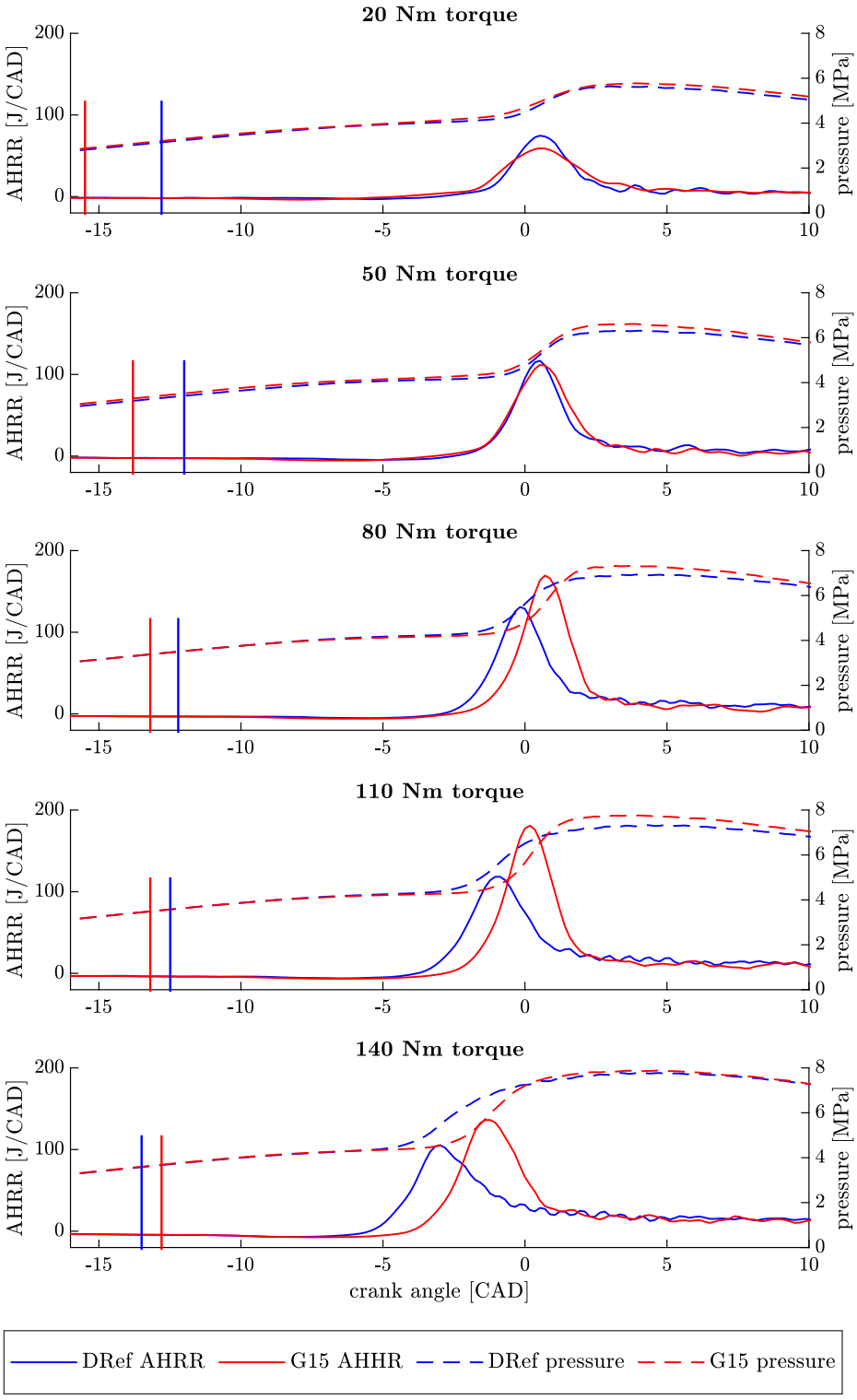

Fig. 4. In-cylinder combustion pressure (right y axis) and apparent heat release rate (left y axis for the DRef and G15, CA50 at 1 CAD aTDC, vertical solids plot lines are the SOI.

with the increase in load (and therefore temperature). This could be due to the longer ignition delay present with G15, hence longer mixing time available, hence large pre-mixed burn fraction with higher AHRR. This result is thought to be due to the lower volatility and lower cetane number of the glycerol.

As shown in Fig. 6, there was no significant impact on the brake thermal efficiency (BTE), with absolute deviations being less than 0.8% across all conditions. Improved brake thermal efficiency of 2% as reported by Sidhu [23] could not be confirmed. The previously detected improvement is assumed to be caused by differences in combustion timing which was not adjusted.

The main difference in engine related measurements between the fuels was the observed CO, THC (see Fig. 7) and the PM emissions. The G15 increased both CO and THC, which matches the behaviour that is observed in previous studies [24,23]. There was twice as much CO emission at the lowest load but the ratio between CO emitted between

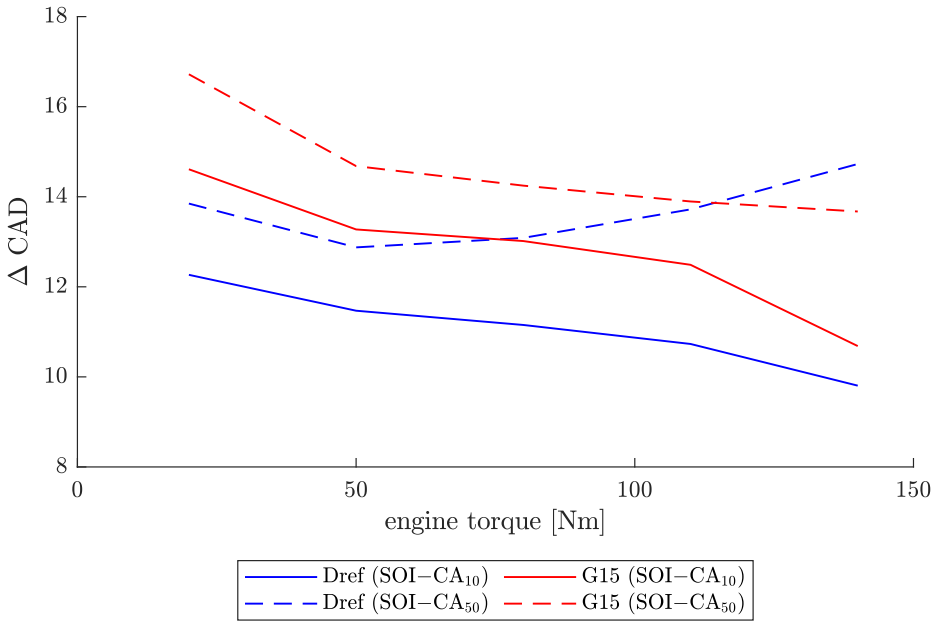

Fig. 5. Time, in CAD between the SOI and CA10 and CA50 for DRef and G15 with varying load.

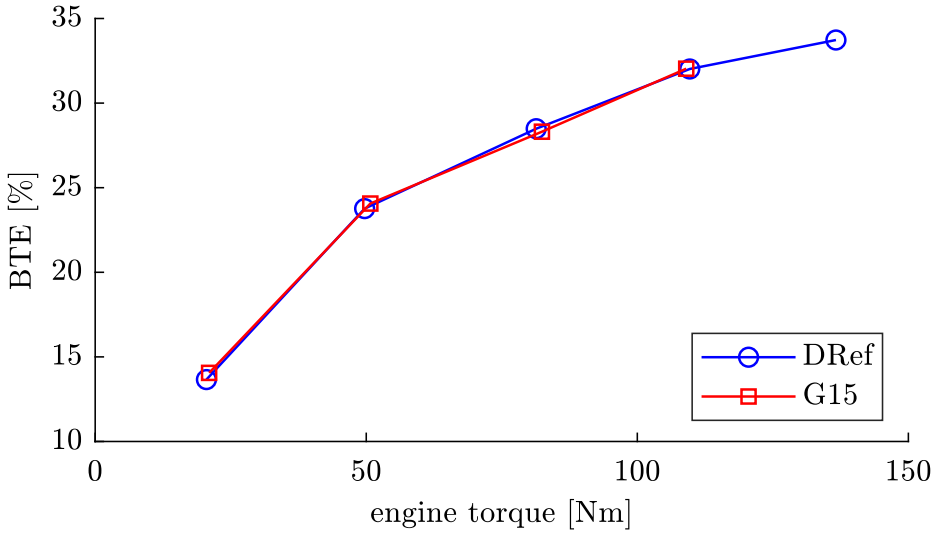

Fig. 6. Engine break thermal efficiency with engine load for DRef and G15.

the fuels decreased with increasing load. The increase in these emissions associated with incomplete combustion is attributed to the low reactivity of glycerol, which has a more profound impact at the lower load conditions where temperatures during the combustion were lower.

The PM size distribution, Fig. 8, includes a very narrow, large peak in the diameter range of 5 to 10 nm for the G15 which is 2 orders of magnitude larger than the number of particles detected in this range for the DRef. No such peak was observed with DRef. The height of this G15 peak increases with engine load, Fig. 8a.

Further investigation of the PM was conducted. PM was sampled onto glass fibre filters at the same location in the exhaust as the DMS was installed with the engine operating at 50 Nm load. The DRef soot collected on the filter was the usual black colour associated with soot, whilst the G15 sample was a mixture of black and brown. This was an early, visual indication that the G15 PM contained a larger fraction of non-soot particles. Both samples were subjected to a thermogravimetric analysis (TGA). The samples were prepared in such a way that the sample placed in the TGA also included some of the glass fiber filter, TGA results are shown in Fig. 9 with the weight normalized to the initial value.

The samples were initially heated under an inert atmosphere (devolatilisation), followed by a cool-down phase, then heated in an oxidant atmosphere (oxidation), full details in the works by Emberson et al. and Rodriguez-Fernandez et al. [28,39]. The largest weight fraction of the sample were glass fibres, which were found to have a weight loss of less than 2% during the thermogravimetric analysis. During devolatilisation, the DRef and the G15 samples lost similar mass until the temperature reaches 100°C, likely caused by moisture evaporation. During devolatilisation the G15 sample mass decreased faster than the DRef sample, leading to a difference in mass loss during the stationary phase at 550°C. This is indicative of a higher semi-volatile (SVOC) organic content in the G15 sample. As the sample loaded into the TGA contains both soot and glass fibre filter and the ratio of soot to filter in each sample is unknown, the mass difference at the end of the devolatilisation phase cannot be used as an indicator of the total difference in SVOC. With the oxidant atmosphere the G15 sample lost mass faster,

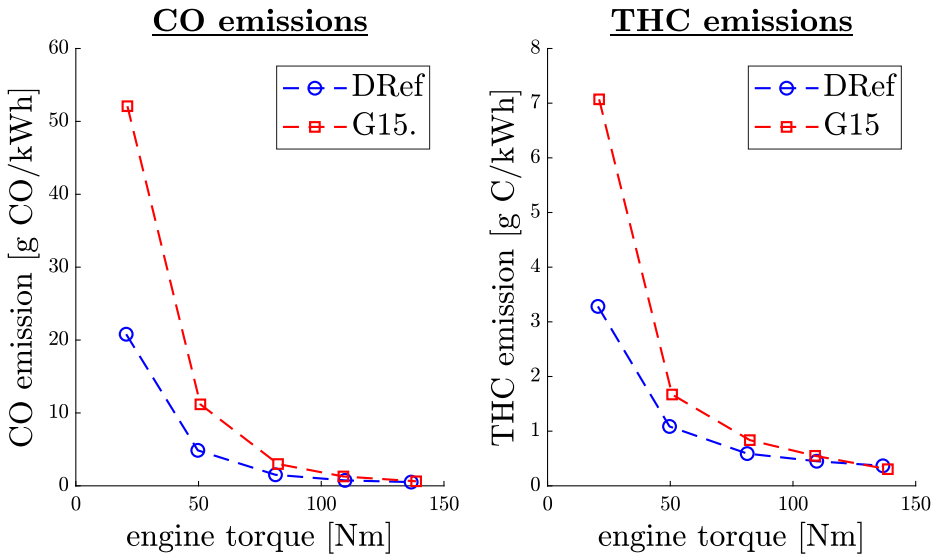

Fig. 7. CO and THC emissions from the instrumented engine for DRef and G15.

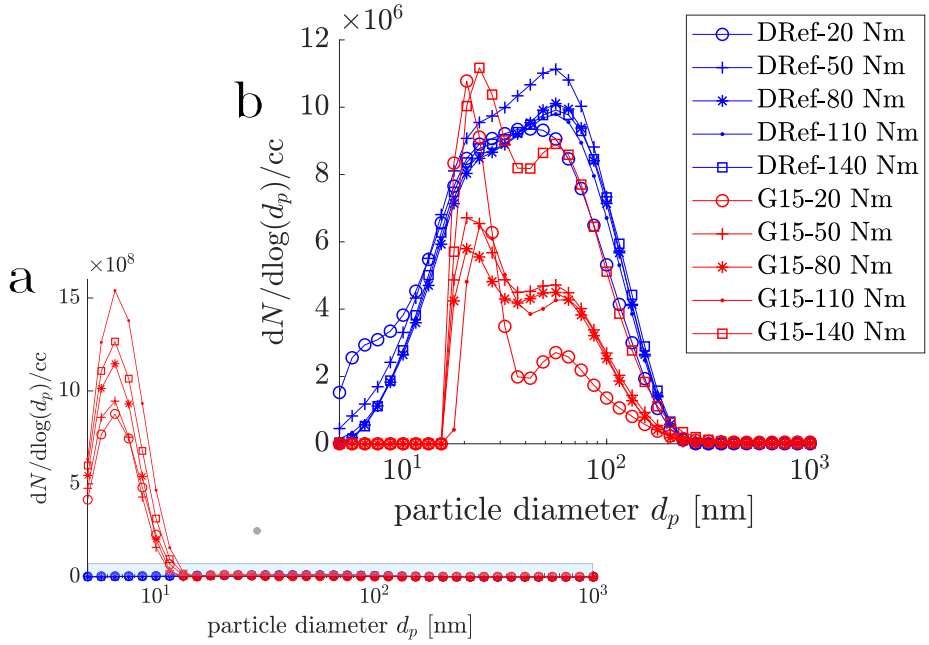

Fig. 8. Particle size distribution (a) scaled to shown peak at small Dp (b) Scaled to show accumulation mode peak.

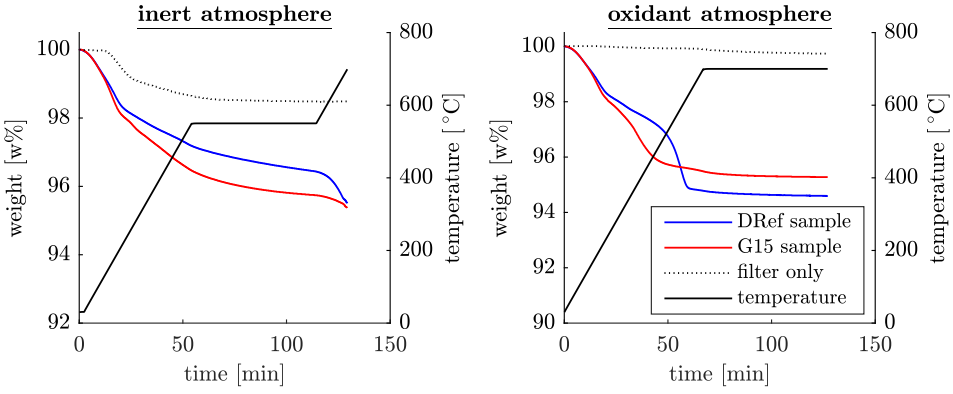

Fig. 9. TGA results of soot under inert and oxidation conditions.

meaning the soot present oxidised at a faster rate than the DRef soot, suggesting it is more reactive.

To compare the samples regarding their SVOC, the ratio between the devolatilisation percentage mass loss (100°C to 550°C) and oxidation percentage mass loss was determined and shown in Table 6.

The higher value for G15 is interpreted as a larger semi-volatile to soot ratio. The large peak of small diameter particles observed in the DMS (Fig. 8a) for G15 is likely to be SVOC nucleation mode particles caused by condensing SVOCs. Another hypothesis is that the small particles may be a result of impurities in the glycerol (technically speaking glycerin), resulting in the glycerol having a higher ash content which would produce a large ash nucleation mode in the same size range. An elemental analysis of the soot and/or glycerin would be the only way to distinguish this and is recommended as further work. In the work [17] crude glycerol was utilised as a boiler fuel with considerable PM emission observed, where the small amount of soluble catalyst left from production was assumed to be responsible. The increase in height of the peak, i.e the increase in the number of the small particles observed with engine load, indicates that the higher temperatures present during combustion do not reduce the number but increase with increasing fuel mass injected. This supports that the higher volume of glycerol being injected at higher loads increases the amount of SVOC through incomplete combustion due to low volatility. If the particles are not condensing SVOCs but small solid soot particles, they are especially harmful due to their penetration ability [40].

By changing the scale of the y-axis (number of particles) of the DMS plot, Fig. 8b the particle numbers in the larger, accumulation mode can be compared. The small particle peak and the accumulation count for G15 are separated, with few particles detected between them. This is highly indicative that the peaks are from a different origin. G15 emits a much smaller number of particles with diameters greater than 25 nm, with a significant drop in the number of particles at around 60 nm. This results in a very different size profile of the accumulation mode G15 compared to the DRef. The reduction in 60 nm PM is largest at low engine loads. The number of particles with diameters greater than 25 nm is reduced by 61% at 20 Nm, by 56% at 80 Nm, and by 11% at 140 Nm. Examining the DMS results, the soot filters and the TGA results shows the G15 has drastically changed the exhaust out PM in quantity, character and size profile. This is most definitely a result of the oxygen content, the low reactivity, lower volatility and the physical fluid properties of the glycerol in the G15.

Brake specific CO and PM emissions are highest at the lowest load condition and decrease with increasing engine torque. Comparing the emissions for each condition, the diesel/glycerol emulsion yields a reduction in PM while increasing CO emissions. While the $PM_{dp>25nm}$ reduction is most effective at low load conditions, the CO increase is likewise. This trade-off is thought to be due to glycerol's low reactivity. As the engine torque is increased and temperatures during combustion increase, the lower reactivity of the glycerol has less of an impact on CO formation. The higher temperatures during the higher torque conditions will also lead to higher rates of soot oxidation in the combustion chamber. If glycerol is reducing soot through its oxygen content, this would be expected to be most evident at the lowest loads where later cycle soot oxidation will be lower. The increase of CO emissions of around 20% at the higher load conditions may be regarded as a minor concern as the absolute value of CO concentrations is very low. In contrast, the increase in CO concentration at the low load condition is critical as the CO concentration is much higher, hence the large $PM_{dp>25nm}$ reduction has to be put into perspective to the significant CO increase.

Table 6
TGA ratios.

Parameter	DRef	G15
$\frac{\Delta w_{inert,100-500^\circ}}{\Delta w_{oxidation}}$	$\frac{3.05\%}{5.41\%} = 0.56$	$\frac{3.73\%}{4.7\%} = 0.79$

3.2. OACIC results

The ignition delay time (IDT) in the OACIC was determined from the time between the initial OH* emission and SOI. SOI was determined from the DBIEI to remove trigger and hydraulic injection delay from the measured IDT. Fig. 10 shows the ignition delay time for both fuels. The error bars represent the 95% confidence interval of the true mean. The ignition delay of G15 was longer than DRef's for all conditions, and the difference did not decrease with rising ambient temperature. This supports the ignition delay times observed in the engine (Fig. 5) where the G15 exhibit longer delay (time to CA10) which did not reduce with increasing temperature (i.e increasing engine load, hence higher temperatures in the combustion chamber, even during injection) apart from at the highest engine load (140 Nm). Whilst the spray, fuel volume injected, and the mixing (due to the engine piston bowl squish zone) is very different in the engine to the chamber, where there is no spray wall interaction, the fuel trend remains. This increased ignition delay time is a consequence of the glycerol high flash point, boiling point and auto igniting temperature.

Ignition delay indicates the time available for fuel and air mixing prior to the premixed combustion phase; the flame lift-off length (FLOL) is an indicator of fuel and air mixing during the mixing-controlled combustion phase. To analyse the behaviour during the mixing-controlled combustion period, the instantaneous FLOL was determined from the integrated OH* intensity in each pixel column. The integrated intensity is calculated in an area close to the centre-line as represented by two white lines in Fig. 11. The instantaneous flame lift-off length is then determined passing a threshold of 0.13 (Fig. 11).

As the slope of cross-sectional integrated OH* intensity is similar for both fuels, the threshold value had little impact on the differences between the fuels. Fig. 12 shows the temporal FLOL averaged over all injections with the coloured shade indicating the 95% confidence interval. After ignition and the premixed period, the FLOL stabilises at a constant level before the end of the injection period. Whilst the fuel sprays ignite downstream of the stable level for Condition 1, they ignite slightly upstream at Condition 3. Increasing ambient temperature results in a decrease of the FLOL for both fuels with differences in FLOL between the fuels becoming very small. Compared to the DRef, the G15 has a 2.5 mm longer FLOL at the low temperature condition, whereas at the high temperature condition both fuels show a very similar FLOL. Based on this FLOL interpretation, the quasi-steady period is identified, beginning at 2.5 ms and ending at 3.8 ms after SOI.

Pickett et al. [41] showed that the ignition quality of a fuel affects lift-off length. In the case of fuels with a big difference in cetane number, fuels with shorter ignition delays generally produced shorter lift-off lengths. However, fuels with a small difference in cetane number and/or containing oxygen do not necessarily show the same trend, as shown by Park et al. and Manin et al. [7,5]; it may be different depending on fuel properties resulting from the components of fuel blends, mixture

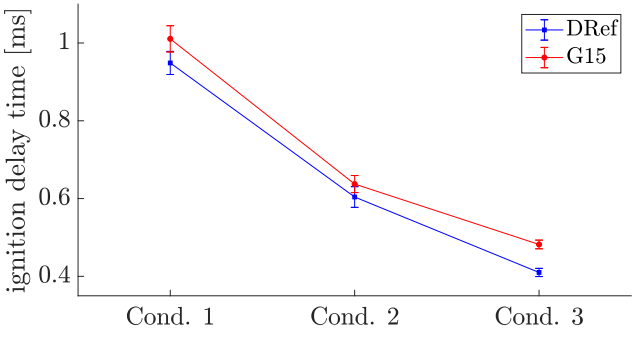

Fig. 10. Ignition delay times for each fuel at each condition.

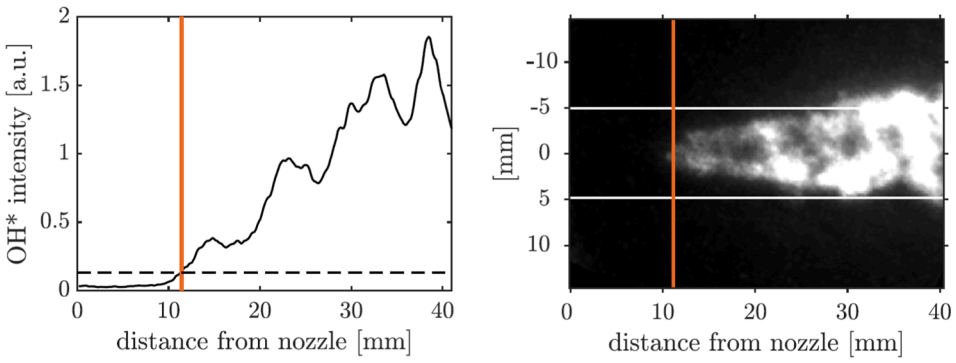

Fig. 11. Exemplary determination of the instantaneous FLOL (red line) by the cross-sectional integrated OH* intensity (solid black line) passing a threshold value (dashed line) (exemplary OH* image on the right side: DRef, Cond.3 Inj. 3 Frame 150).

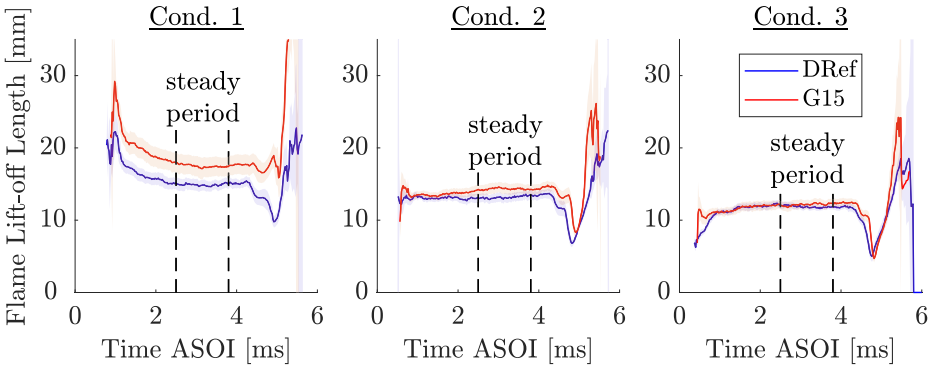

Fig. 12. FLOL with time ASOI for each fuel at each condition with the quasi-steady period bracketed by the dashed black lines.

ratios or injection velocities. The similarity in the FLOL at Cond.2 and Cond.3 for the two fuels suggest similar upstream mixing is available for both fuels.

The DBI, light extinction measurements are divided into a pre-mixed and quasi-steady phases as the tip of the combustion plume travels outside of the observable area of the OACIC, thus the peak KL value from the total soot in the spray flame may not be determined. As the evaluation of the total soot mass formed was not possible, the soot behaviour is assessed as a spatial soot gradient (SSG) during the quasi-steady combustion period at a fixed distance either from the injector or the FLOL position. A similar technique was previously used by the authors in [30], assuming that the speed of the combustion plume is similar for all fuels, the SSG is an indicative parameter of the soot formation in the flame. To determine the SSG, KL is integrated in each pixel column and plotted over the distance from the injector nozzle. Fig. 13 illustrates the average over all 30 injections of this cross-sectional integrated value as a solid line with the shaded area representing the 95% confidence interval for each fuel. Describing the plot from the injector nozzle on-wards, the initial increase in KL is the light extinction caused by the spray liquid fuel core, which is increasing in the beginning because of the divergence of the spray and decreasing further downstream due to fuel evaporation. It is evident that the G15 has a larger KL spray value at Cond.1 and projects slightly further from the injector tip than the DRef, with the difference reducing at Cond.2 and, by Cond.3 the difference has almost disappeared. This is a direct influence of the higher boiling point of the glycerol present in the G15. Progressing away from the injector tip

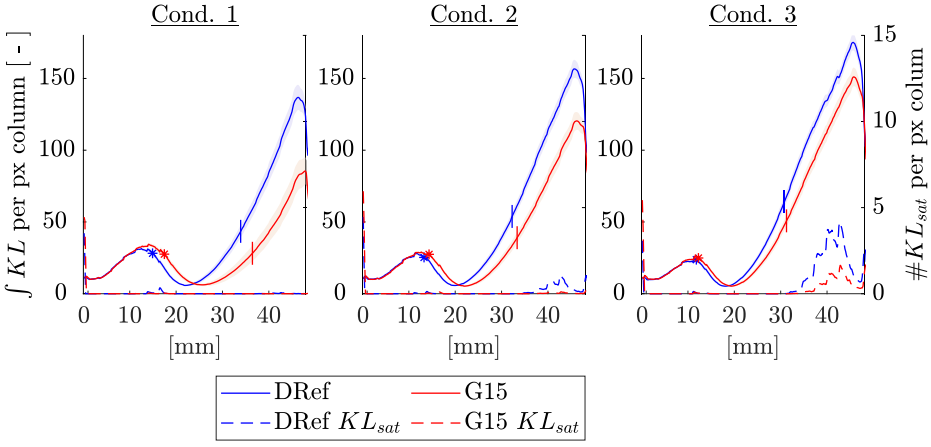

Fig. 13. Integrated KL per pixel column (solid line) and number of saturated KL values per pixel column (dashed line) during the quasi-steady phase for condition 2, with the star representing the FLOL and the vertical line showing 19 mm after FLOL.

results in a reduction in the KL after the spray liquid fuel core peak, with a minimum, that is also positioned further from the tip for G15 at Cond.1, less so at Cond.2 and at the same position for Cond.3. The increase after the minimum indicates the increasing soot concentration with increasing distance from the injector nozzle. KL saturation occurs, which is indicated by the dashed line that illustrates the number of KL saturated pixels per column. DRef and the G15 at Cond.3 are not reliable after 32 mm from injector nozzle. The drop in the cross-sectional integrated KL at the end is caused by the circular chamber wall reducing the observable area.

With rising temperatures, soot is observed closer to the injector and the spatial gradient increases for both fuels. For all conditions the DRef has the biggest increase. A single value metric, the spatial soot gradient (SSG) is the maximum increase of soot mass between the FLOL and 19 mm after the FLOL (19 mm chosen to remove erroneous data due to KL saturation).

By relating the SSG to the FLOL instead of the injector nozzle, the variation of the flame location is taken into account. In Fig. 13 the FLOL is marked with a star and the location of 19 mm after the FLOL is indicated by the vertical line. The change of soot mass is calculated over $\Delta x = 1.63$ mm, in order to smooth out large pixel to pixel fluctuation (see Eq. 5).

$$SSG = max\left(\frac{m_{soot}(x) - m_{soot}(x - \Delta x)}{\Delta x}\right) \quad (5)$$

Fig. 14 shows the averaged KL image over the quasi-steady period with the SSG being displayed at the bottom. Pixels with KL saturation are omitted in the construction of the averaged image.

Fig. 15 shows the SSG plotted against the FLOL. The bars represent the 95% confidence interval of each quantity. For both fuels, the SSG increases with shorter FLOL. A more significant difference between the G15 and the DRef is observed at Cond.1. The G15 has an increased flame lift-off length and a significantly lower SSG. The decrease in SSG is consistent over all conditions, although the differences in FLOL decrease with rising ambient gas temperatures. This indicates that the soot reduction effect of the glycerol is not only physically (mixing) driven as even when the FLOL are similar at Cond.3, the G15 SSG is smaller.

For G15 at Cond.2and Cond.3, the FLOL is similar to the DREf at Cond.1 and Cond.2. The SSG for the two fuels is similar when the FLOL for each fuel is similar, however the ambient gas temperature and pressure and not the same. The higher temperature, Cond.3-G15 and lower temperature, Cond.2-DRef have similar SSG and FLOL. The Cond.3-G15 is producing less soot (lower SSG) likely to be caused by the oxygen content of the glycerol.

The relationship between the OACIC conditions and the engine are not straight forward. The in-flame soot for the G15 can be summarized as being lower than the DRef. The engine out soot, i.e particles measured in the DMS above 10 nm, was reduced with the G15 as well. So the OACIC and engine results are supportive of each other in terms of the soot. The very large sub 10 nm peak seen with G15 in the DMS results, if

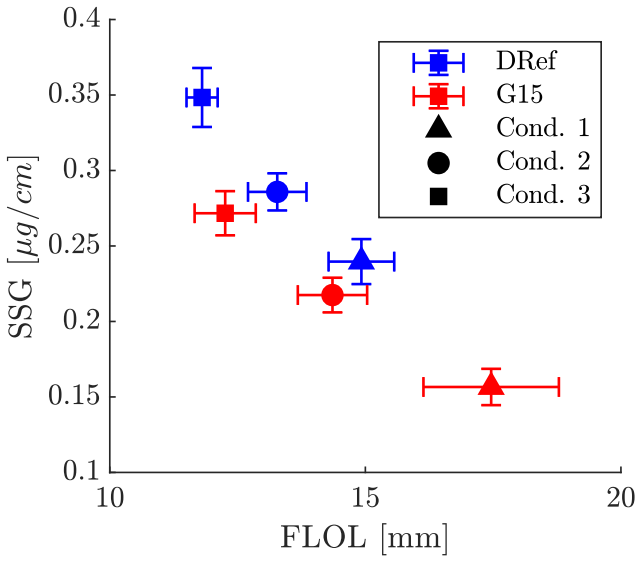

Fig. 15. FLOL vs SSG.

mainly an effect of low fuel volatility, would be expected to be observed in increased liquid length; this does in fact occur at Cond.1, less so at Cond.2 and not at all in Cond.3. Volatility effects on FLOL are difficult to fully distinguish due to other ignition effects on FLOL but it is likely partially the reason for the longer FLOL of the G15 at Cond.1.

3.3. Chemical kinetic results

The combustion chemistry of glycerol has not been studied in great detail; some aspects of its oxidation and pyrolysis were investigated by Hemings et al. [36], Fantozzi et al. [42] and Yuan et al. [43]. The initial steps of soot formation during the combustion process is the production of soot precursors and inline with the hypothesis of this study, glycerol addition to diesel should also exhibit a reduction in their concentration. To this end, zero dimensional constrained pressure ignition calculations with and without glycerol addition to n–heptane, which is chosen to represent diesel fuel in kinetic simulations, were conducted. In here, n–heptane is not meant to represent EN590 rather a general diesel like fuel with high reactivity. There are several studies which have identified these precursors as C2H2, C2H4, PC3H4, C3H6 and have explained in detail how they lead to the eventual inception of soot particles [44,45,35,45]. In addition to these precursors, we have also analyzed the concentrations of CO and CO2 as they were measured during the experiments and are an indicator of progress of the combustion process.

It must be made clear that the chemical kinetic analysis presented in this study is not meant to replace detailed reactive flow analysis considering fuel volatility and diffusion effects, rather it is provided to

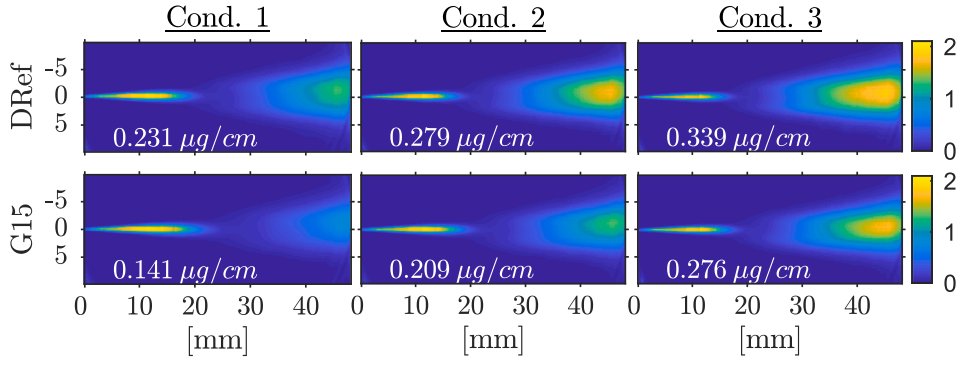

Fig. 14. Averaged KL plots during the quasi-steady period with the bottom value indicating the soot gradient between the white lines.

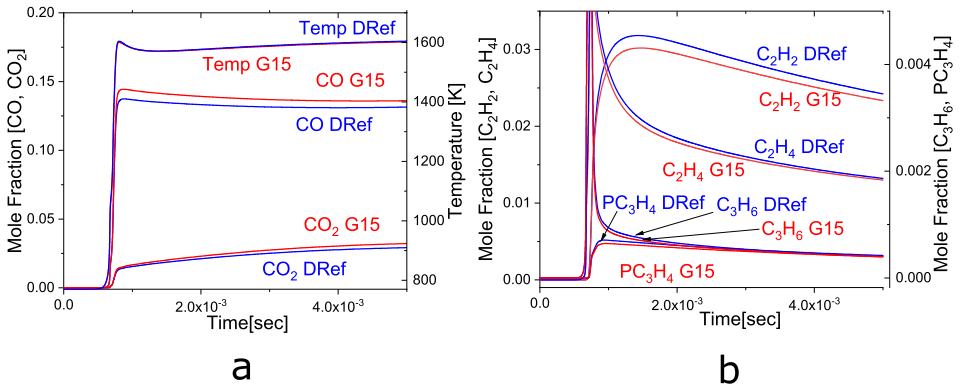

Fig. 16. Results from chemical kinetic simulations (a) CO and CO2 concentrations with time, (b) soot precursor concentrations with time.

explain the effect of glycerol addition on gas phase chemistry. For the initial conditions of simulation, both the mixtures exhibit an onset of ignition at the same time (0.7 ms) and attain roughly the same final temperature. Since the simulations were at such rich conditions, the burnt gases final temperature is much below the adiabatic flame temperature. The concentrations of CO and CO2 emanating from these cases are shown in Fig. 16.a, where the concentration of CO emission is higher in the cases with glycerol present in the fuel, which is consistent with experimental observation shown in Fig. 7. The higher presence of CO indicates towards incomplete combustion due to lower Cetane number or higher octane number of glycerol. This observation is supported by the presence of higher total unburned hydrocarbon concentration in the case of diesel/glycerol emulsion in Fig. 7.

The concentration of soot precursors was also observed during the ignition process and is presented in Fig. 16.b. The species presented in Fig. 16.b are ethene (C2H4), ethyne (C2H2), propyne (PC3H4) and propene (C3H6). These species are shown to be critical to PAH growth and hence contribute significantly towards soot inception. Among these species ethyne is known to be highest contributor towards soot growth [44,45,35,45]. In Fig. 16.b shows the evolution of the species starting with the onset of ignition and peaking shortly after the ignition event. The concentration of these species then reduces slowly with time. The concentrations at the end of the simulation time are taken as the final concentration of these precursors. The results of the simulations indicate that the reduction in concentration of C2H2 and C2H4 is due to the glycerol addition to diesel, however the concentration of C3H6 and PC3H4 were not significantly affected. As earlier explained by Westbrook et al. [34] the oxygenated additives reduce soot by introducing species containing carbon atoms bonded to oxygen atom into the system which do not contribute to PAH chemistry and secondly they also introduce additional oxygen atoms which increase the oxidation of species pool including the soot precursors.

4. Conclusions and summary

This study explores the combustion of diesel and a diesel/glycerol emulsion in two compression ignition combustion systems with multiple diagnostic techniques. Combustion feasibility in a six cylinder CI engine was first conducted. This established that the diesel/glycerol emulsion could be used as a fuel in the engine. Performance, cylinder pressure, AHRR and emissions were observed at different loads at 1800 rpm with combustion phasing so CA50 occurred at 1 CAD aTDC. The PM/soot was measured and analyzed using a DMS 500 and TGA to gather understanding of size distribution. The fuels were also tested in an optically accessible compression ignition combustion chamber to study in-flame soot formation, lift-off length and ignition delay. Three ambient gas conditions (Cond.1, Cond.2 and Cond.3) were used, with constant density; increasing pressure and temperature. To further understand the combustion, a fundamental chemical kinetic study of the diesel/glycerol emulsion, examining the effect of glycerol addition on soot precursor formation was conducted. The collective observations from these studies include:

- Glycerol is not readily miscible with diesel and has to be used as emulsion, a surfactant mixture of Span 80 and Tween 80, with overall HLB of 6.4 was used, according to previous works. The emulsion shown limited stability compared to previous works and started to break after 30 min.
- Emulsions made with ultrasound and the engine fuel mixing were comparable and very similar in visually appearance and viscosity.
- Diesel/glycerol emulsion had longer ignition delay (time SOI to CA10) but higher AHRR with increasing load (time SOI to CA50).
- There was no impact on the brake thermal efficiency with the diesel/glycerol emulsion.
- CO and THC were higher with diesel/glycerol emulsion but the difference became very small as the load, hence temperatures, were increased.
- Diesel/glycerol emitted a smaller number of particles with diameters greater than 25 nm, with a significant drop in the number of particles at 60 nm. The reduction in 60 nm PM is largest at low engine loads. The number of particles with diameters greater than 25 nm is reduced by 61% at 20 nm, by 56% at 80 Nm, and by 11% at 140 Nm.
- A large peak of sub 10 nm particles, 2 orders of magnitude greater than with diesel alone, is observed in the DMS results for diesel/glycerol emulsion. This is hypothesised to be semi-volatile organic compounds that have started to condense in the exhaust and DMS. These SVOCs are present in the exhaust gas due to the low volatility of the glycerol in the emulsion.
- The larger fraction of SVOC in the exhaust is supported by the TGA analysis of the soot collected on a filter which has a ratio between the devolatilisation percentage mass loss (100°C to 550°C) and oxidation percentage mass loss of 0.56 for diesel fuel and 0.79 for diesel/glycerol emulsion, interpreted as a larger semi-volatile to soot ratio.
- Ignition delay time, determined from the OH* flame emission, was always longer for the diesel/glycerol emulsion at all conditions.
- In-flame soot, as indexed by the spatial soot gradient (SSG) was always lower with the diesel/glycerol emulsion at all conditions. Flame lift-off length decreased with increasing temperate and pressure of the ambient gas whilst SSG increased. Flame lift-off length of the diesel/glycerol was longer at the lower temperature condition.
- The concentration of known soot precursors, C2H2 and C2H4 was reduced due to glycerol addition but the concentrations of C3H6 and PC3H4 were not significantly affected.

CRediT authorship contribution statement

David Robert Emberson: Conceptualization, Methodology, Writing - original draft, Writing - review & editing, Supervision. **Jan Wyndorps:**

Investigation, Software, Formal analysis, Writing - original draft. **Ahfaz Ahmed:** Methodology, Investigation. **Karl Oskar Pires Bjørgen:** Methodology, Software, Data curation. **Terese Løvås:** Software, Project administration, Funding acquisition.

Declaration of Competing Interest

The authors declare that they have no known competing financial interests or personal relationships that could have appeared to influence the work reported in this paper.

Acknowledgements

The research reported in this work was supported by Bio4Fuels (FME) of the Research Council of Norway, Project Number 257622.

References

[1] Stamatellou A-M, Stamatelos A. Overview of diesel particulate filter systems sizing approaches. Appl Therm Eng 2017;121:537–46.
[2] Zhu X, Andersson Öivind. Performance of new and aged injectors with and without fuel additives in a light duty diesel engine. Transp Eng 2020;1:100007.
[3] Verma P, Jafari M, Rahman SA, Pickering E, Stevanovic S, Dowell A, Brown R, Ristovski Z. The impact of chemical composition of oxygenated fuels on morphology and nanostructure of soot particles. Fuel 2020;259:116167.
[4] Guan C, Cheung C, Li X, Huang Z. Effects of oxygenated fuels on the particle-phase compounds emitted from a diesel engine. At Pollution Res 2017;8(2):209–20.
[5] Manin J, Skeen S, Pickett L, Kurtz E, Anderson JE. Effects of oxygenated fuels on combustion and soot formation/oxidation processes. Int Powertrains, Fuels Lubricants Meeting 2014;3(7):704–17.
[6] Mueller CJ, Pitz WJ, Pickett LM, Martin GC, Siebers DL, Westbrook CK. Effects of oxygenates on soot processes in di diesel engines: experiments and numerical simulations. SAE Trans 2003:964–82.
[7] Park W, Park S, Reitz RD, Kurtz E. The effect of oxygenated fuel properties on diesel spray combustion and soot formation. Combust Flame 2017;180:276–83.
[8] Verma P, Stevanovic S, Zare A, Dwivedi G, Chu Van T, et al., An overview of the influence of biodiesel, alcohols, and various oxygenated additives on the particulate matter emissions from diesel engines, Energies 12 (10).
[9] Song J, Cheenkachorn K, Wang J, Perez J, Boehman AL, Young PJ, Waller FJ. Effect of oxygenated fuel on combustion and emissions in a light-duty turbo diesel engine. Energy Fuels 2002;16(2):294–301.
[10] Nabi MN, Kannan D, KannanJohan D, Hustad EHE, Rahman MM. Role of oxygenated fuel to reduce diesel emissions: A review. In: Proceedings of the International Conference on Mechanical Engineering; 2009.
[11] Guarieiro LLN, de Almeida Guerreiro ET, dos Santos Amparo KK, Manera VB, Regis ACD, Santos AG, et al. Assessment of the use of oxygenated fuels on emissions and performance of a diesel engine. Microchem J 2014;117:94–9.
[12] Emberson DR, Bjorgen KO, Lovas T, Arctic biodiesel performance and pm number emissions, The Proceedings of the International symposium on diagnostics and modeling of combustion in internal combustion engines (2017) C205.
[13] Leung DY, Wu X, Leung M. A review on biodiesel production using catalyzed transesterification. Appl Energy 2010;87(4):1083–95.
[14] Quispe CA, Coronado CJ, Jr JAC. Glycerol Production, consumption, prices, characterization and new trends in combustion. Renew Sustain Energy Rev 2013;27:475–93.
[15] Coronado CR, Carvalho JA, Quispe CA, Sotomonte CR. Ecological efficiency in glycerol combustion. Appl Therm Eng 2014;63(1):97–104.
[16] Fernando S, Adhikari S, Kota K, Bandi R. Glycerol based automotive fuels from future biorefineries. Fuel 2007;86(17):2806–9.
[17] Steinmetz SA, Herrington JS, Winterrowd CK, Roberts WL, Wendt JO, Linak WP. Crude glycerol combustion: Particulate, acrolein, and other volatile organic emissions. Proc Combust Inst 2013;34(2):2749–57.
[18] Melero JA, Vicente G, Morales G, Paniagua M, Bustamante J. Oxygenated compounds derived from glycerol for biodiesel formulation: Influence on EN 14214 quality parameters. Fuel 2010;89(8):2011–8.
[19] Cornejo A, Barrio I, Campoy M, Lázaro J, Navarrete B. Oxygenated fuel additives from glycerol valorization. main production pathways and effects on fuel properties and engine performance: A critical review. Renew Sustain Energy Rev 2017;79:1400–13.
[20] Szoeri M, Giri BR, Wang Z, Dawood AE, Viskolcz B, Farooq A. Glycerol carbonate as a fuel additive for a sustainable future. Sustainable Energy Fuels 2018;2:2171–8.
[21] Okoye P, Abdullah A, Hameed B. Synthesis of oxygenated fuel additives via glycerol esterification with acetic acid over bio-derived carbon catalyst. Fuel 2017;209:538–44.
[22] Samoilov V, Maximov A, Stolonogova T, Chernysheva E, Kapustin V, Karpunina A. Glycerol to renewable fuel oxygenates. part i: Comparison between solketal and its methyl ether. Fuel 2019;249:486–95.
[23] Sidhu MS, Roy MM, Wang W. Glycerine emulsions of diesel-biodiesel blends and their performance and emissions in a diesel engine. Appl Energy 2018;230:148–59.
[24] Eaton SJ, Harakas GN, Kimball RW, Smith JA, Pilot KA, Kuflik MT, Bullard JM. Formulation and combustion of glycerol–diesel fuel emulsions. Energy Fuels 2014;28(6):3940–7.
[25] McNeil J, Day P, Sirovski F. Glycerine from biodiesel: The perfect diesel fuel. Process Saf Environ Prot 2012;90(3):180–8.
[26] Setyawan HY, Zhu M, Zhang Z, Zhang D. Ignition and combustion characteristics of single droplets of a crude glycerol in comparison with pure glycerol, petroleum diesel, biodiesel and ethanol. Energy 2016;113:153–9.
[27] Debnath BK, Saha UK, Sahoo N. A comprehensive review on the application of emulsions as an alternative fuel for diesel engines. Renew Sustain Energy Rev 2015;42:196–211.
[28] Emberson DR, Rohani B, Wang L, Saeterli R, Lovas T, On soot sampling: considerations when sampling for tem imaging and differential mobility spectrometer. In: 14th International Conference on Engines & Vehicles, SAE International; 2019.
[29] Elsanusi OA, Roy MM, Sidhu MS. Experimental investigation on a diesel engine fueled by diesel-biodiesel blends and their emulsions at various engine operating conditions. Appl Energy 2017;203:582–93.
[30] Bjorgen KO, Emberson DR, Lovas T. Optical measurements of in-flame soot in compression-ignited methyl ester flames. Energy Fuels 2019;33(8):7886–900.
[31] Choi MY, Mulholland GW, Hamins A, Kashiwagi T. Comparisons of the soot volume fraction using gravimetric and light extinction techniques. Combust Flame 1995;102(1):161–9.
[32] Bjørgen KOP, Emberson DR, Lovas T, Diffuse back-illuminated extinction imaging of soot: effects of beam steering and flame luminosity. In: International Powertrains, Fuels & Lubricants Meeting, SAE International; 2019.
[33] Higgins B, Siebers DL, Measurement of the flame lift-off location on di diesel sprays using oh chemiluminescence. In: SAE 2001 World Congress, SAE International; 2001.
[34] Westbrook CK, Pitz WJ, Curran HJ. Chemical kinetic modeling study of the effects of oxygenated hydrocarbons on soot emissions from diesel engines. J Phys Chem A 2006;110(21):6912–22.
[35] Frenklach M, Wang H. Detailed modeling of soot particle nucleation and growth. Symp (Int) Combust 1991;23(1):1559–66.
[36] Hemings EB, Cavallotti C, Cuoci A, Faravelli T, Ranzi E. A detailed kinetic study of pyrolysis and oxidation of glycerol (propane-1,2,3-triol). Combust Sci Technol 2012;184(7–8):1164–78.
[37] Curran H, Gaffuri P, Pitz W, Westbrook C. A comprehensive modeling study of n-heptane oxidation. Combust Flame 1998;114(1):149–77.
[38] Yang W, An H, Chou S, Chua K, Mohan B, et al. Impact of emulsion fuel with nano-organic additives on the performance of diesel engine. Appl Energy 2013;112:1206–12.
[39] Rodríguez-Fernández J, Oliva F, Vázquez RA. Characterization of the diesel soot oxidation process through an optimized thermogravimetric method. Energy Fuels 2011;25(5):2039–48.
[40] Steiner S, Bisig C, Petri-Fink A, Rothen-Rutishauser B. Diesel exhaust: current knowledge of adverse effects and underlying cellular mechanisms. Arch Toxicol 2016;90:1541–53.
[41] Pickett LM, Siebers DL, Idicheria CA, Relationship between ignition processes and the lift-off length of diesel fuel jets. In: Powertrain & Fluid Systems Conference & Exhibition, SAE International; 2005.
[42] Fantozzi F, Frassoldati A, Bartocci P, Cinti G, Quagliarini F, Bidini G, Ranzi E. An experimental and kinetic modeling study of glycerol pyrolysis. Appl Energy 2016;184:68–76.
[43] Yuan X, Leng L, Xiao Z, Lai C, Jiang L, Wang H, et al. Pyrolysis and combustion kinetics of glycerol-in-diesel hybrid fuel using thermogravimetric analysis. Fuel 2016;182:502–8.
[44] Haynes B, Wagner H. Soot formation. Prog Energy Combust Sci 1981;7(4):229–73.
[45] Wagner H. Soot formation in combustion. Symp (Int) Combust 1979;17(1):3–19.